

# Control-oriented modeling of two-phase flow and input/output structures for boundary control

Snezana Djordjevic<sup>1,2</sup>, Okko H. Bosgra<sup>1,2</sup>, Paul M.J. Van den Hof<sup>1</sup>,  
Dimitri Jeltsema<sup>3</sup>

<sup>1</sup>Delft Center for Systems and Control, Delft University of Technology, The Netherlands

<sup>2</sup> Control Systems Technology Group, Eindhoven University of Technology, The Netherlands

<sup>3</sup> Delft Institute of Applied Mathematics, Delft University of Technology, The Netherlands

## Abstract

This paper develops a control-oriented modeling approach to two-phase flow systems. The control-oriented two-phase flow model is established based on a set of simplified relationships of the exact physical modeling with respect to the spatial domain, which include one-dimensional (1D) approximation and approximation of the coupling terms between the phases. The derived control-oriented two-phase flow model is governed by a set of partial differential algebraic equations (PDAEs) that describes the propagation of fluid fractions and mixture velocity in 1D, and can be used to control the flow by manipulation of the boundary conditions. The key element in our work is the linearized model representation of the two-phase flow written in the Laplace-space domain that connects the two-phase flow regimes and input/output structures. Using the input/output structures, which have to satisfy causality conditions, the two-phase flow can be regulated by applying a boundary controller. The advantage of the Laplace-space approach and the effectiveness of the proposed boundary control design are illustrated with a numerical example of a counter-current two-phase flow in a vertical bubble column.

## 1 Introduction

Under the influence of unprecedented market demands in the petroleum, pharmaceutical, food, and cosmetic industries, the chemical industry has evolved considerably over the last two decades. Following the demands and achievements made in these fields, plant capacities have greatly increased, incorporating new technologies to support the enlargement. New technologies originate from different fields such as: material science (e.g., safe construction of large-size reactors and pipes), mechanical engineering (e.g., construction of agitators that enhance the mixing of reactants), chemical engineering (e.g., decreasing process time and increasing productivity), and control engineering (e.g., safe regulation of pressure and temperature inside the reactors). Due to the complex nature of the chemical processes and equipment designs, the ability to build plants “a bit bigger” is slowly reaching its limitations [5]. Operating the large-scale plants in an optimal and safe manner is becoming almost

impossible for some production processes (e.g., mixing inside large-scale reactors, transportation of fluid in long pipelines, distribution of particles in crystallizers, or pressure distribution in distillation columns). This dictates a growing need to replace current large, expensive, and energy-intensive equipment with smaller, less costly, and more efficient equipment for a production process [24, 31]. The production-related problems in the large-scale plants cannot be effectively solved with the current reactor design and are still not scaled-up to the optimal volume. The scale-up technology is twofold and involves the design and optimal operation of a chemical process. Obviously, the design has important consequences for chemical engineering such as process modeling or process systems control. In this sense, the model development and inclusion of innovative types of equipment in process design play a crucial role in future developments. In order to be able to replace the current large-scale equipment and to scale-up a plant more efficiently, a better understanding and more accurate models of chemical process are needed to accurately predict the behavior of the processes and to enable control of the processes.

A significant problem in modeling of chemical processes is the occurrence of transport phenomena such as fluid flow that lead to low efficiency at larger scales. The benefit for the chemical industry that can be gained from applying a flow control strategy to intensify the chemical processes is enormous. The problem of controlling and modeling the fluid flow systems is, however, extremely complex and involved. For flow control of single-phase flow systems, we refer to [3, 1, 20]. Concerning the modeling of multiphase flow systems, many contributions have been presented in the multiphase flow community, ranging from fundamental studies [9, 17] to studies focused on specific two-phase flow regimes [4, 28, 16, 11]. Most of these currently used two-phase flow models require complex algorithms such as computational fluid dynamics (CFD), due to the complex nature of the governing equations [18]. Despite the fact that there is a large number of CFD models in the multiphase flow community, there is a common agreement that the pure two-phase fluid transport has to be governed by a set of first-order hyperbolic PDEs [28, 17, 25]. Essentially, this means that the transport phenomena of the two-phase flow represent delays of the fluid properties from one point in space to another, whereas the interactive terms between the phases represent dissipation and/or instabilities of the flow. This is an important aspect of the two-phase flow as it gives a new perspective on the two-phase flow control. The first step in this direction has been presented in [14] where 1D two-phase flow hyperbolic-like PDE model was derived for flow control.

In the control community, first-order hyperbolic PDE models have been widely studied over the last two decades. The examples include control methods for heating in reactors [29, 7, 23], flow in tubular reactors [32, 12, 10], and open channel flow [10]. The conventional approach to PDE models is to discretize the model equations in space and then apply control theory for ODE systems [8], or alternatively to derive an analytical solution of a PDE model and apply spatially distributed controllers [21, 6]. Recent results extend the existing control approaches to the stabilization of the hyperbolic PDE systems, proposing a frequency domain approach to control the hyperbolic PDE systems [22]. This frequency approach to fluid flow systems gives an input/output description of the fluid flow. The work presented in [22] demonstrates the usefulness of the classical frequency approach and functional relationships for analysis and control of a channel flow system represented by a set of hyperbolic PDEs. The frequency approach to fluid flow systems eventually leads to

an easy-to-implement algorithm for the fluid flow control and does not rely on the accuracy of the chosen discretization method [13].

In this paper, we introduce a theoretical framework for deriving a control-oriented two-phase flow mode based on the Laplace transformation of the governing hyperbolic-like PDEs [14]. The main contribution is in the Laplace-space representation of the two-phase flow model, which links the flow regimes and causal input/output structures. From the derived causal input/output structures, the boundary control design then easily follows.

## 2 The control-oriented two-phase flow model

### 2.1 Two-phase flow

Many examples involving two-phase fluid systems appear in the chemical industry, such as the partial oxidation of ethylene to acetaldehyde (i.e., the Wacker-Hoechst process) or the carbonization of methanol to acetic acid. Other occurrences of two-phase flow appear in the injection of steam into oil wells for enhanced oil recovery, in the condensation of higher hydrocarbons, in natural gas pipelines due to low temperatures of surrounding air or soil, in a boiling water nuclear reactor, in fluidized beds, and in fermentors for the production of enzymes and drugs. For a more extensive overview, we refer to [11].

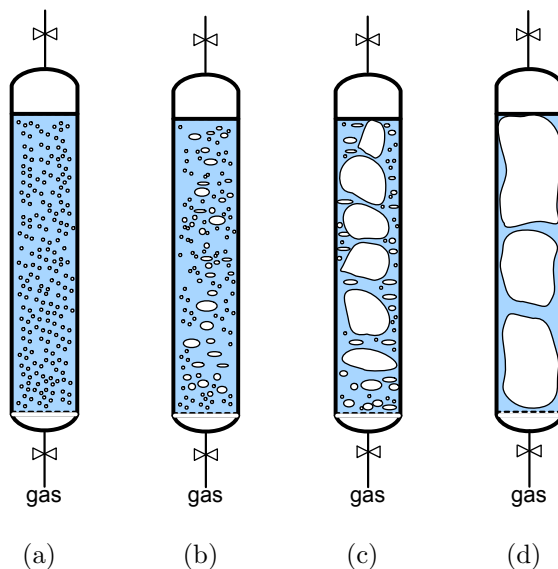


Figure 1: Flow patterns of a vertical upward flow in a bubble column: (a) bubble, (b) bubble-slug transition, (c) slug, and (d) annular.

All these processes take place in reactors that are often referred to as bubble column reactors. As shown in Figure 1, a bubble column reactor is a vertical cylinder, where a gas phase enters at the bottom of the column through a gas distributor. The column is filled with liquid which expands under the influence of the gas injection. Different flow regimes can be created on the microscopic scale depending on the magnitude of the gas injection. Figure

1 shows different flow regimes and levels of coalescence of bubbles present in the column. In the bubble flow, the gas consists of discrete bubbles immersed in the liquid phase that moves against the gas flow. Increasing the gas injection at the bottom of the column, these small bubbles coalesce into slugs. The transition from bubble flow (Figure 1(a)) towards annular flow (Figure 1(d)) depends on the size of the bubbles, injection techniques, and surface-tension effects. The large number of bubbles, which can coalesce into slugs, increases the gas volume fraction and decreases the presence of the liquid phase. Consequently, the gap between the gas and the wall narrows, and the downward flow dominates the column. This causes a rather strong relative velocity between the gas and the liquid phase.

As shown in Figure 1(c), the coalescing effect inside the bubble column can be observed only on the microscopic scale. On the reactor scale, the coalescing of the bubbles into slugs is mainly observed in decreased mass rates due to the small contact area between the gas and the liquid phase. In principle, the bubble column reactor is characterized by a lack of any mechanical means of agitation, and the mixing is carry on by motion of the fluid phases. For this reason, bubble flow is particularly efficient for mixing which can increase transfer rates due to the large contact area between the phases. The transfer rates are mainly determined by the size of the contact area and the circulation rates of the liquid and gas phase, and can be increased by enlarging the contact area between the phases. A poor liquid circulation has an adverse effect on the transfer rate and the residence time of the gas phase, whereas a well-circulated liquid phase increases the reactor volume. In reactor design, the main objective is to keep a large contact area between the phases while maintaining an ideal balance between these two extreme circulation phenomena.

## 2.2 1D two-phase flow model

In order to develop a comprehensive strategy for a two-phase flow system inside a reactor column, the first step is to define a set of assumptions needed to simplify the flow problem. The following assumptions have been made for deriving a control-oriented microscopic two-phase flow model based on microscopic conservation laws:

1. The fluids (gas and liquid) are considered to be incompressible.
2. The entire volume is occupied by gas and liquid, which is defined by the volume fractions of the gas phase  $\alpha_g$  and the liquid phase  $\alpha_l$ , and for each volume element  $\alpha_g + \alpha_l = 1$  holds.
3. The flow over the entire cross section is uniform, i.e., the flow variations occur only in 1D.
4. The gas phase is dispersed and consists of bubbles which are spherical in shape and uniform in size. The processes of coalescence and breakage are neglected.
5. No mass transfer occurs between the two phases.
6. Each phase is treated as a continuum in the spatial domain under consideration.
7. In each volume element, there is a sufficiently large number of bubbles that create the continuum gas phase.

8. The pressure influence is modeled by distinguishing a bulk pressure and an interfacial pressure.
9. The pressure in each volume element is proportional to the fractional area occupied by the phases.
10. The interfacial tension also causes the pressure  $\Delta p_g$  for the tension from the gas side, and  $\Delta p_l$  for the tension from the liquid side at the surface.
11. The drag force is considered to be the only coupling term between the phases; all the other coupling terms are neglected.

According to the given assumptions, a 1D form of the microscopic conservation laws can be obtained using the following set of PDEs for the mass conservation laws

$$\frac{\partial \alpha_g}{\partial t} + \frac{\partial \alpha_g}{\partial x} v_g + \alpha_g \frac{\partial v_g}{\partial x} = 0, \quad (1)$$

$$\frac{\partial \alpha_l}{\partial t} + \frac{\partial \alpha_l}{\partial x} v_l + \alpha_l \frac{\partial v_l}{\partial x} = 0, \quad (2)$$

and the following set of PDEs for the momentum conservation laws

$$\alpha_g \rho_g \frac{\partial v_g}{\partial t} + \alpha_g v_g \rho_g \frac{\partial v_g}{\partial x} + \alpha_g \frac{dp}{dx} + \Delta p_g \frac{\partial \alpha_g}{\partial x} = -\alpha_g \rho_g g - F, \quad (3)$$

$$\alpha_l \rho_l \frac{\partial v_l}{\partial t} + \alpha_l v_l \rho_l \frac{\partial v_l}{\partial x} + \alpha_l \frac{dp}{dx} + \Delta p_l \frac{\partial \alpha_l}{\partial x} = -\alpha_l \rho_l g + F, \quad (4)$$

where  $\rho_g$  is the density of the gas phase,  $\rho_l$  is the density of the liquid phase,  $v_g$  is the velocity of the gas phase, and  $v_l$  is the velocity of the liquid phase, with  $F$  as the coupling force. In principle, the balance equations are derived for each phase separately, which are coupled via interactive terms [15]. Many of the presently used two-phase flow models use different interfacial coupling forces with sometimes ambiguous physical background and empirical closure equations [19]. Thus, we consider only the most dominant coupling term which is the drag force

$$F = F_d = \beta (v_g - v_l),$$

closed by the following equation

$$\beta = \frac{3C_d}{4d_b} \alpha_g \alpha_l \rho_l |v_g - v_l|,$$

where  $C_d$  is the drag coefficient and  $d_b$  is the diameter of a single bubble.

In deriving the momentum balance equations, we use the interfacial pressures  $\Delta p_g$  and  $\Delta p_l$  in (3) and (4) respectively. Since the interfacial pressures are functions of  $v_g$  and  $v_l$ , they can also be considered as coupling terms. The liquid interfacial pressure can be obtained from the following expression

$$\Delta p_l = C_p \alpha_l \rho_l (v_g - v_l)^2,$$

where  $C_p$  is the interfacial pressure coefficient [28], whereas the gas pressure difference  $\Delta p_g$  can be neglected due to the low density of the gas phase.

As far as the total pressure is concerned, the momentum balance equations (3) and (4) share the pressure term proportional to the gas fractions. This fact can be used to derive a more compact representation of the two-phase flow. The pressure term can be eliminated by dividing (3) and (4) by  $\alpha_g$  and  $\alpha_l$ , respectively, and subtracting one from the other. Under the conditions  $\alpha_g \neq 0$  and  $\alpha_l \neq 0$ , we can obtain the total momentum equation of the two-phase flow system as

$$\begin{aligned} \rho_g \frac{\partial v_g}{\partial t} - \rho_l \frac{\partial v_l}{\partial t} + \rho_g v_g \frac{\partial v_g}{\partial x} - \rho_l v_l \frac{\partial v_l}{\partial x} + C_p \rho_l (v_g - v_l)^2 \frac{\partial \alpha_g}{\partial x} \\ = -(\rho_g - \rho_l)g - (v_g - v_l) \left( \frac{\beta}{\alpha_g} + \frac{\beta}{\alpha_l} \right). \end{aligned} \quad (5)$$

Equation (5) describes the total momentum of the mixture with no pressure variation outside the system boundaries. The signs in front of the time derivatives can be assigned to the direction of the fluid velocities.

Before writing the final form of the two-phase flow model, we can make one more simplification step. Due to the assumption that a volume is occupied with gas and liquid, i.e.,  $\alpha_g + \alpha_l = 1$ , (2) can be rewritten in terms of  $\alpha_g$  only as

$$\frac{\partial(1 - \alpha_g)}{\partial t} + \frac{\partial(1 - \alpha_g)}{\partial x} v_l + (1 - \alpha_g) \frac{\partial v_l}{\partial x} = 0. \quad (6)$$

After rearranging, (6) reads as

$$\frac{\partial \alpha_g}{\partial t} + \frac{\partial \alpha_g}{\partial x} v_l - (1 - \alpha_g) \frac{\partial v_l}{\partial x} = 0. \quad (7)$$

The last step includes subtracting (1) from (7). Now, the final set of PDEs can be written as

$$\begin{aligned} \frac{\partial \alpha_g}{\partial t} + \frac{\partial \alpha_g}{\partial x} v_g + \alpha_g \frac{\partial v_g}{\partial x} &= 0, \\ \rho_g \frac{\partial v_g}{\partial t} - \rho_l \frac{\partial v_l}{\partial t} + \rho_g v_g \frac{\partial v_g}{\partial x} - \rho_l v_l \frac{\partial v_l}{\partial x} + C_p \rho_l (v_g - v_l)^2 \frac{\partial \alpha_g}{\partial x} \\ &= -(\rho_g - \rho_l)g - (v_g - v_l) \left( \frac{\beta}{\alpha_g} + \frac{\beta}{1 - \alpha_g} \right), \\ \frac{\partial \alpha_g}{\partial x} (v_g - v_l) + \frac{\partial v_g}{\partial x} \alpha_g + (1 - \alpha_g) \frac{\partial v_l}{\partial x} &= 0, \end{aligned}$$

which in a compact form reads as

$$\mathbf{E} \frac{\partial \Phi}{\partial t} + \mathbf{A}(\Phi) \frac{\partial \Phi}{\partial x} = \mathbf{c}(\Phi), \quad (8)$$

where  $\Phi = [\alpha_g \ v_g \ v_l]^T$  is the vector of fluid variables. The matrices

$$\mathbf{E} = \begin{bmatrix} 1 & 0 & 0 \\ 0 & \rho_g & -\rho_l \\ 0 & 0 & 0 \end{bmatrix}, \quad (9)$$

and

$$\mathbf{A}(\Phi) = \begin{bmatrix} v_g & \alpha_g & 0 \\ C_p \rho_l (v_g - v_l)^2 & \rho_g v_g & -\rho_l v_l \\ v_g - v_l & \alpha_g & 1 - \alpha_g \end{bmatrix}, \quad (10)$$

are the system matrices, and

$$\mathbf{c}(\Phi) = \begin{bmatrix} 0 \\ -(\rho_g - \rho_l)g - (v_g - v_l) \left( \frac{\beta}{\alpha_g} + \frac{\beta}{1-\alpha_g} \right) \\ 0 \end{bmatrix} \quad (11)$$

is the coupling force vector. A similar set of simplification steps has been published in [25] where the coupling forces between the phases were studied using a two-phase flow model for adiabatic two-phase bubble flow. The interfacial momentum exchange in [25] includes the surface stress developed on the interface which is induced by the relative motion of the phases, interfacial pressure, and the drag force. In this work, we focus on the drag force and interfacial pressure only for incompressible two-phase fluid flow systems.

### 2.3 Well-posedness of the model formulation

One of the first steps in deriving a control-oriented two-phase flow model is to verify the well-posedness of the model formulation and to classify the derived partial differential algebraic equations (PDAE) model, suggesting well-posed initial-boundary conditions. The physical intuition of the well-posed PDAE problem formulation suggests that the well-posed problem has a unique solution for time-dependent problems. Parabolic and hyperbolic PDAE models are known to be well-posed problems with a stable and unique solution, whereas elliptic PDAE models are ill-posed with a solution that propagates in all directions which is characteristic of time independent problems, i.e., static potential problems. In general, an ill-posed problem usually means that the PDAE has to be solved backwards in time domain, which is not physically possible, and therefore it represents ill-posed model formulations.

In principle, the nature of possible solutions to (8) is characterized by the coefficients of the characteristic polynomial obtained from the system matrices of the derived model (9) and (10), which describes the fluid flow phenomena. For the PDAE model given by (8), the degree of the characteristic polynomial is smaller than or equal to the number of states. This means that the eigenvalues corresponding to the algebraic part have eigenvalues with infinitely many solutions, and the eigenvalues with the finite solutions correspond to the dynamical part. For the model given as (8), the eigenvalue analysis shows that the system has one infinite eigenvalue and two finite eigenvalues which can be obtained from the characteristic polynomial

$$\det(\lambda \mathbf{E} - \mathbf{A}(\Phi)) = a_1 \lambda^2 + a_2 \lambda + a_3, \quad (12)$$

where

$$\begin{aligned} a_1 &= -\alpha_g \rho_l - \rho_g + \rho_g \alpha_g, \\ a_2 &= 2 \rho_g v_g - 2 v_g \rho_g \alpha_g + 2 \alpha_g \rho_l v_l, \\ a_3 &= -C_p \rho_l (v_g - v_l)^2 \alpha_g^2 + (\rho_g v_g^2 - \rho_l v_l^2 + C_p \rho_l (v_g - v_l)^2) \alpha_g - \rho_g v_g^2. \end{aligned}$$

The discriminant of (12) is then defined by

$$D_c = a_2^2 - 4a_1a_3. \quad (13)$$

Since  $\alpha_g < 1$ , the discriminant is negative, i.e.,  $D_c < 0$  for all values of the velocities  $v_g$  and  $v_l$ . After deriving the characteristic polynomial (12), we can directly obtain the eigenvalues of (8) from the following expressions

$$\lambda_1(\Phi) = \frac{\alpha_g \rho_l v_l + \alpha_l \rho_g v_g}{\alpha_g \rho_l + \alpha_l \rho_g} + \sqrt{D_c}, \quad (14)$$

$$\lambda_2(\Phi) = \frac{\alpha_g \rho_l v_l + \alpha_l \rho_g v_g}{\alpha_g \rho_l + \alpha_l \rho_g} - \sqrt{D_c}. \quad (15)$$

These eigenvalues represent the characteristic velocities of the gas/liquid phase in the two-phase fluid flow system. Due to the fact that  $\rho_g > 0$  and  $\rho_l > 0$ , the signs of the eigenvalues change according to the velocities  $v_g$  and  $v_l$ . The results of the eigenvalues and the range of the velocities for which the model is well-posed are given in Table 1. In the range outside the given velocity ratios, the model is ill-posed. In Figure 2, we present an analysis of the characteristic polynomial for  $\alpha_g = 0.1$ ,  $\rho_g = 1 \text{ kg/m}^3$ , and  $\rho_l = 1000 \text{ kg/m}^3$  in order to illustrate the velocity influence on the eigenvalues.

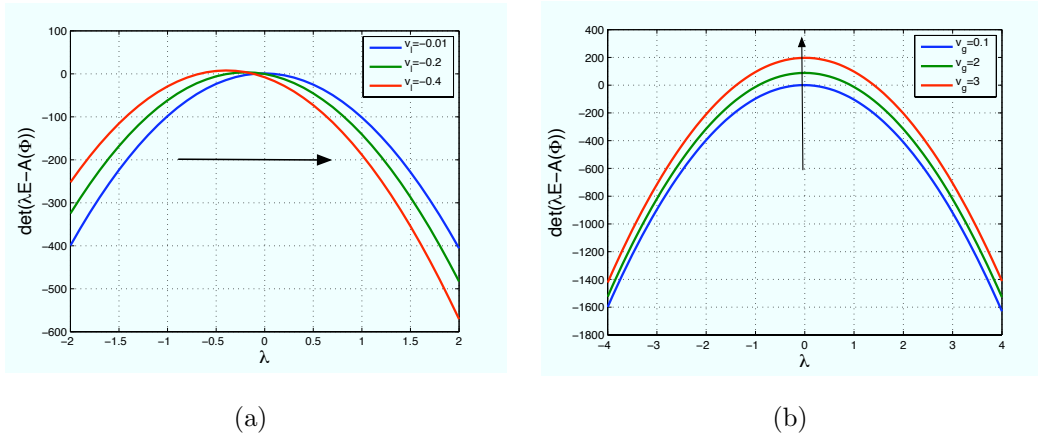


Figure 2: Influence of the velocities  $v_g$  and  $v_l$  on the characteristic polynomial with the eigenvalues determined by  $\det(\lambda \mathbf{E} - \mathbf{A}(\Phi)) = 0$  for (a)  $v_g = 0.2 \text{ m/s}$  and (b)  $v_l = -0.02 \text{ m/s}$ .

If  $D_c > 0$ , the system (8) is said to be hyperbolic. The eigenvalues of the hyperbolic equations are real and distinct. If  $D_c = 0$ , the system is parabolic with real repeated eigenvalues. If  $D_c < 0$ , the system is elliptic with complex eigenvalues. Elliptic systems with one coordinate being time is inherently non-causal, and for that reason is ill-posed. For modeling, it means that the assumptions used to derive the model are not correct. In general, elliptic system with one coordinate being time are proven to be ill-posed, whereas parabolic and hyperbolic systems are well-posed with a stable and unique solution [27, 28]. In order to define a critical point between the well-posed and ill-posed solutions to the two-phase flow

Table 1: Well-posed regions of the two-phase flow model based on the eigenvalues (14) and (15) for a wide range of the velocities  $v_g$  and  $v_l$ , where  $\alpha_g = 0.1$ ,  $\rho_g = 1 \text{ kg/m}^3$ , and  $\rho_l = 1000 \text{ kg/m}^3$ .

Eigenvalues	Velocity conditions obtained from (14) and (15)	Ratio between the velocities
$\lambda_1 = \lambda_2$	$-0.45v_g + 1.45v_l =$ $= 0.47v_g + 0.53v_l$	$v_l/v_g = 1$
$\lambda_1 > 0$ $\lambda_2 > 0$	$v_l/v_g > -0.89$ $v_l/v_g > 0.3$	$v_l/v_g > 0.3$
$\lambda_1 < 0$ $\lambda_2 > 0$	$v_l/v_g > -0.89$ $v_l/v_g < 0.3$	$-0.89 < v_l/v_g < 0.3$
$\lambda_1 < 0$ $\lambda_2 < 0$	$v_l/v_g < -0.89$ $v_l/v_g < 0.3$	$v_l/v_g > -0.89$

model (8), we evaluate (13) as

$$D_c = D \left( 1 - \left( \frac{\rho_l \alpha_g + \alpha_l \rho_g}{\rho_g} \right) C_p \right), \quad (16)$$

where  $D = \alpha_g \rho_g \rho_l (v_g - v_l)^2 (-1 + \alpha_g)$ . Since  $\alpha_g < 1$ , then for all values of the velocities  $v_g$  and  $v_l$  the discriminant is negative, i.e.,  $D < 0$ . This implies that the well-posedness of the PDAE model (8) is determined by the interfacial pressure coefficient  $C_p$ . The critical  $C_p$ , for which the discriminant  $D_c = 0$  and the system is parabolic, can be obtained from the system parameters  $\rho_g$  and  $\rho_l$ , and the volume fraction  $\alpha_g$  as

$$C_p = \frac{\rho_g}{\alpha_g \rho_l + \rho_g \alpha_l}.$$

There have been many studies over the last two decades focusing on the interfacial pressure coefficient  $C_p$  for different fluid systems [19]. For the air-water system, the interfacial pressure coefficient  $C_p$  is reported to be between 0.25 and 0.5 [25]. For this value of  $C_p$ , the derived two-phase flow model (8) is in the hyperbolic region for a wide range of gas fractions  $\alpha_g$  (see Table 1), and (8) is valid for that region only.

## 2.4 Linearized two-phase flow model

Suppose that  $\bar{\Phi}$  is a steady-state solution of the derived two-phase flow model (8), and  $\Phi'$  is a small perturbation around the steady-state solution, then the flow variable  $\Phi$  can be written as

$$\Phi = \bar{\Phi} + \Phi', \quad (17)$$

and the linearized two-phase flow model can be defined as

$$\mathbf{E} \frac{\partial \Phi'}{\partial t} + \mathbf{A}(\bar{\Phi}) \frac{\partial \Phi'}{\partial x} + \bar{\mathbf{A}}(\Phi') \frac{\partial \bar{\Phi}}{\partial x} = \mathbf{F} \Phi', \quad (18)$$

with

$$\mathbf{A}(\bar{\Phi}) = \begin{bmatrix} \bar{v}_g & \bar{\alpha}_g & 0 \\ C_p \rho_l (\bar{v}_g - \bar{v}_l)^2 & \rho_g \bar{v}_g & -\rho_l \bar{v}_l \\ \bar{v}_g - \bar{v}_l & \bar{\alpha}_g & 1 - \bar{\alpha}_g \end{bmatrix},$$

$$\bar{\mathbf{A}}(\Phi') = \begin{bmatrix} v_g' & \alpha_g' & 0 \\ 2C_p \rho_l (\bar{v}_g - \bar{v}_l) (v_g' - v_l') & \rho_g v_g' & -\rho_l v_l' \\ v_g' - v_l' & \alpha_g' & -\alpha_g' \end{bmatrix},$$

representing the linearized system matrices, and

$$\mathbf{F} = \begin{bmatrix} 0 & 0 & 0 \\ 0 & -3/2 \frac{C_d \rho_l \sqrt{(\bar{v}_g - \bar{v}_l)^2}}{db} & 3/2 \frac{C_d \rho_l \sqrt{(\bar{v}_g - \bar{v}_l)^2}}{db} \\ 0 & 0 & 0 \end{bmatrix}$$

representing the linearized force vector. The derivation of (18) is given in Appendix A. Essentially, the space-dependent steady-state solutions represent the flow patterns in the observed domain. If there is no variation of the steady-state solution with respect to space, i.e.,  $\bar{\Phi} = \text{const}$ , the linearized two-phase flow model reduces to the following equation

$$\mathbf{E} \frac{\partial \Phi'}{\partial t} + \mathbf{A}(\bar{\Phi}) \frac{\partial \Phi'}{\partial x} = \mathbf{F} \Phi'. \quad (19)$$

In order to demonstrate the linearization technique while enforcing the well-posedness of the model formulation, simulations are carried out using a space-independent steady-state solution i.e., quasi steady-state solution. The quasi steady-state solution, which is spatially uniform, can be used as an equilibrium point for the linearization of the two-phase flow model. Section 3 will discuss the possible quasi steady-state solutions and their physical interpretations.

## 2.5 Coordinate transformations

In this section, we use the linearized two-phase flow model (19) to reformulate the linear PDAE problem into a linear PDE using standard coordinate transformation techniques. It is important to emphasize that the coordinate transformations do not change the system dynamics, instead with the coordinate transformation the model is represented by another coordinate system. The linearized two-phase flow model written as a linear PDE model is rather beneficial for control designs, which will be illustrated in Section 5.1.

Here, we introduce two sets of coordinate transformations: one that eliminates the algebraic part of the linearized two-phase flow model (19), and one that decouples the characteristic wave velocities  $\lambda_1(\bar{\Phi})$  and  $\lambda_2(\bar{\Phi})$ . The first coordinate transformation is introduced in order to simplify the computations involving the algebraic equation in the linear PDAE model (19). For that, the system matrix  $\mathbf{E}$  in (19) has to be diagonalized, so that in the new coordinate system the linearized PDAE model (19) can be reduced by eliminating the

algebraic equation. This means that the system can be decomposed into the dynamic and algebraic part by diagonalizing  $\mathbf{E}$ . Using the following coordinate transformation

$$\mathbf{T} = \begin{bmatrix} 1 & 0 & 0 \\ 0 & \rho_g^{-1} & \rho_l \\ 0 & 0 & \rho_g \end{bmatrix},$$

the state vector  $\Phi'$  can be transformed into a new state vector  $\Psi'$  such that according to the given fluid variables  $\Phi' = [\alpha'_g \ v'_g \ v'_l]^T$ , the new states read as

$$\Psi' = \mathbf{T}^{-1}\Phi' = \begin{bmatrix} \alpha'_g \\ \rho_g v'_g - \rho_l v'_l \\ \frac{v'_l}{\rho_g} \end{bmatrix},$$

and the diagonalizing  $\mathbf{E}$  reads as

$$\mathbf{E}\mathbf{T} = \begin{bmatrix} 1 & 0 & 0 \\ 0 & 1 & 0 \\ 0 & 0 & 0 \end{bmatrix}.$$

The two-phase flow model in the new coordinates  $\Psi'$  can be written as

$$\mathbf{E}\mathbf{T} \frac{\partial \Psi'}{\partial t} + \mathbf{A}(\overline{\Psi'}) \mathbf{T} \frac{\partial \Psi'}{\partial x} = \mathbf{F}\mathbf{T}\Psi'. \quad (20)$$

Here, we present a symbolic representation of the linearized model<sup>1</sup>, and later on we will present some numerical results. We start with the two-phase flow model (19) in the coordinates  $\Psi'$

$$\begin{bmatrix} 1 & 0 & 0 \\ 0 & 1 & 0 \\ 0 & 0 & 0 \end{bmatrix} \frac{\partial \Psi'}{\partial t} + \begin{bmatrix} \overline{v}_g & \frac{\overline{\alpha}_g}{\rho_g} & \overline{\alpha}_g \rho_l \\ C_p \rho_l (\overline{v}_g - \overline{v}_l)^2 & \overline{v}_g & \rho_g \overline{v}_g \rho_l - \rho_l \overline{v}_l \rho_g \\ \overline{v}_g - \overline{v}_l & \frac{\overline{\alpha}_g}{\rho_g} & \overline{\alpha}_g \rho_l + (1 - \overline{\alpha}_g) \rho_g \end{bmatrix} \frac{\partial \Psi'}{\partial x} = \begin{bmatrix} 0 & 0 & 0 \\ 0 & -\frac{3}{2} \frac{C_d \rho_l \sqrt{(\overline{v}_g - \overline{v}_l)^2}}{d_b \rho_g} & -\frac{3}{2} \frac{C_d \rho_l^2 \sqrt{(\overline{v}_g - \overline{v}_l)^2}}{d_b} + \frac{3}{2} \frac{C_d \rho_l \sqrt{(\overline{v}_g - \overline{v}_l)^2} \rho_g}{d_b} \\ 0 & 0 & 0 \end{bmatrix} \Psi', \quad (21)$$

where the state  $\Psi'_3$  can be obtained from the last equation in (21) as

$$\frac{\partial \Psi'_3}{\partial x} = \frac{(\rho_g \overline{v}_g - \rho_g \overline{v}_l)}{\rho_g (-\overline{\alpha}_g \rho_l - \rho_g + \rho_g \overline{\alpha}_g)} \frac{\partial \Psi'_1}{\partial x} + \frac{\overline{\alpha}_g}{\rho_g (-\overline{\alpha}_g \rho_l - \rho_g + \rho_g \overline{\alpha}_g)} \frac{\partial \Psi'_2}{\partial x}. \quad (22)$$

<sup>1</sup>The notation  $(\cdot)'$  is used to emphasize the linear approximation of the nonlinear two-phase flow model written in different coordinate systems.

After the elimination of  $\Psi'_3$ , the system takes the following form

$$\frac{\partial}{\partial t} \begin{bmatrix} \Psi'_1 \\ \Psi'_2 \end{bmatrix} + \mathbf{A}_{\text{red}} \frac{\partial}{\partial x} \begin{bmatrix} \Psi'_1 \\ \Psi'_2 \end{bmatrix} = \mathbf{F}_{\text{red}} \begin{bmatrix} \Psi'_1 \\ \Psi'_2 \end{bmatrix}. \quad (23)$$

with

$$\mathbf{A}_{\text{red}} = \begin{bmatrix} \frac{-\rho_g \bar{v}_g + \bar{v}_g \rho_g \bar{\alpha}_g - \bar{\alpha}_g \rho_l \bar{v}_l}{-\bar{\alpha}_g \rho_l - \rho_g + \rho_g \bar{\alpha}_g} & \frac{\bar{\alpha}_g (-1 + \bar{\alpha}_g)}{-\bar{\alpha}_g \rho_l - \rho_g + \rho_g \bar{\alpha}_g} \\ \frac{(\bar{v}_g - \bar{v}_l)^2 \rho_l (-C_p \rho_l \bar{\alpha}_g + \rho_g \bar{\alpha}_g C_p + \rho_g - \rho_g C_p)}{-\bar{\alpha}_g \rho_l - \rho_g + \rho_g \bar{\alpha}_g} & \frac{-\rho_g \bar{v}_g + v_{gi} \rho_g \bar{\alpha}_g - \bar{\alpha}_g \rho_l \bar{v}_l}{-\bar{\alpha}_g \rho_l - \rho_g + \rho_g \bar{\alpha}_g} \end{bmatrix},$$

and

$$\mathbf{F}_{\text{red}} = \begin{bmatrix} 0 & 0 \\ -\frac{3}{2} \frac{C_d \rho_l (\bar{v}_g - \bar{v}_l) (-\rho_l \bar{v}_g + \rho_l \bar{v}_l + \rho_g \bar{v}_g - \rho_g \bar{v}_l)}{d_b (-\bar{\alpha}_g \rho_l - \rho_g + \rho_g \bar{\alpha}_g)} & -\frac{3}{2} \frac{C_d \rho_l (\bar{v}_g - \bar{v}_l)}{d_b (-\bar{\alpha}_g \rho_l - \rho_g + \rho_g \bar{\alpha}_g)} \end{bmatrix},$$

where  $\mathbf{A}_{\text{red}}$  has the same eigenvalues as the pair  $(\mathbf{A}(\Phi), \mathbf{E})$ .

Now, we will introduce the second coordinate transformation which is used to decouple the directional derivatives  $\frac{\partial \Psi'}{\partial x}$  as to diagonalize  $\mathbf{A}_{\text{red}}$ . First, we introduce the following coordinate transformation

$$\Psi' = \mathbf{V} \mathbf{W}',$$

where  $\mathbf{V}$  is the transformation matrix that gives

$$\frac{\partial \mathbf{V} \mathbf{W}'}{\partial t} + \mathbf{A}_{\text{red}} \frac{\partial \mathbf{V} \mathbf{W}'}{\partial x} = \mathbf{F}_{\text{red}} \mathbf{V} \mathbf{W}', \quad (24)$$

which reads as follows in the new coordinate system  $\mathbf{W}'$

$$\frac{\partial \mathbf{W}'}{\partial t} + \mathbf{V}^{-1} \mathbf{A}_{\text{red}} \mathbf{V} \frac{\partial \mathbf{W}'}{\partial x} = \mathbf{V}^{-1} \mathbf{F}_{\text{red}} \mathbf{V} \mathbf{W}'. \quad (25)$$

Equation (25) describes the linearized two-phase flow model written as the PDE with the decoupled wave propagation. The final form of the linearized two-phase flow model with the decoupled directional derivatives can be written as

$$\frac{\partial}{\partial t} \begin{bmatrix} W'_1 \\ W'_2 \end{bmatrix} + \begin{bmatrix} \lambda_1 & 0 \\ 0 & \lambda_2 \end{bmatrix} \frac{\partial}{\partial x} \begin{bmatrix} W'_1 \\ W'_2 \end{bmatrix} = \begin{bmatrix} c_{11} & c_{12} \\ c_{21} & c_{22} \end{bmatrix} \begin{bmatrix} W'_1 \\ W'_2 \end{bmatrix}. \quad (26)$$

Due to the model simplicity given in the  $\mathbf{W}'(t, x)$  coordinate system, (26) is well-suited for a boundary control that will be discussed in Section 5. Essentially, the applied transformations represent a permutation of the model equations written in a compact matrix form, involving a full state transformation. In the case of full state transformation of  $\Phi'(t, x)$ , the new states  $\mathbf{W}'(t, x)$  cannot be associated with physical states any more, but the relationships between new and old states are fixed by the transformation matrices  $\mathbf{T}$  and  $\mathbf{V}$ . Although the main purpose of the coordinate transformation presented in this section is to decouple the directional derivatives that lead to the determination of a well-posed boundary actuation strategy, the coordinate transformations also suggest a well-suited numerical scheme for spatial discretization of (26). This has been discussed in [30].

## 3 Operational regimes

### 3.1 Steady-state solutions

As discussed in Section 2.1, there is a wide range of possible operational regimes in a bubble column [11]. For example, the bubble column reactor in a homogeneous regime is characterized by a more or less uniform gas volume fraction distribution within the reactor, whereas a heterogeneous regime is characterized by a non-uniform distribution and an internal re-circulation of the phases (see Figure 1). This means that a steady-state solution is space-dependent for the non-uniform flow, whereas for the uniform flow the gas distribution is constant in the entire space:  $\bar{\Phi} = \text{const}$ . This space-independent steady-state solution will be called a quasi steady-state solution. In the quasi steady-state situation, the gravitational force and the drag force are in balance, and the flow is uniform through the whole domain  $[0, L]$  as illustrated in Figure 3. The figure also illustrates two different flow regimes that often appear in bubble columns. Figure 3(a) illustrates a co-current flow, while Figure 3(b) illustrates a counter-current flow. The distinction between those flows is based on the direction of the phase velocities. Roughly speaking, if both phases move upwards (i.e., from bottom to top), the flow is considered to be co-current; whereas for fluid systems in which the phases move in opposite directions, the flow is considered to be counter-current. To determine the direction of the velocities in the quasi steady-state regime, we introduce a slip velocity  $v_s$  as a difference between the velocity of the gas phase and the velocity of the liquid phase  $v_s = v_g - v_l$ . According to the definition of the slip velocity and relationship between  $v_g$  and  $v_l$ , we can obtain the following expression from the momentum equations (3) and (4):

$$v_s = \sqrt{\frac{4(\rho_l - \rho_g)gd_b(1 - \alpha_g)}{3C_d\rho_l}}.$$

To determine the gas and liquid velocities  $v_g$  and  $v_l$  in the quasi steady-state regime, we need an additional relation that will link  $v_g$  and  $v_l$ . The additional equation can be obtained from the volumetric fluxes across the volume section. For the bubble column with an open flow through the boundaries illustrated in Figure 3, the compensating volumetric flux across the volume in the quasi steady-state equals zero, i.e.,

$$\alpha_g v_g + \alpha_l v_l = 0.$$

In this case, the velocity of each phase can be computed as

$$\begin{aligned} v_g &= \alpha_l v_s, \\ v_l &= -\alpha_g v_s. \end{aligned}$$

In the case of real flows, a certain amount of fluid moves downwards and a certain amount moves upwards. For the 1D two-phase flow, the liquid velocity simply represents a sum of the upwards and downwards flow:

$$v_l^{\text{down}} + v_l^{\text{up}} = v_l.$$

Which of the two liquid velocities is more dominant depends on the gas and liquid injection techniques at the boundaries. In Section 5.1, we will illustrate the use of the quasi steady-state operational regimes in analyzing the boundary conditions, which leads to the development of well-posed actuation strategies.

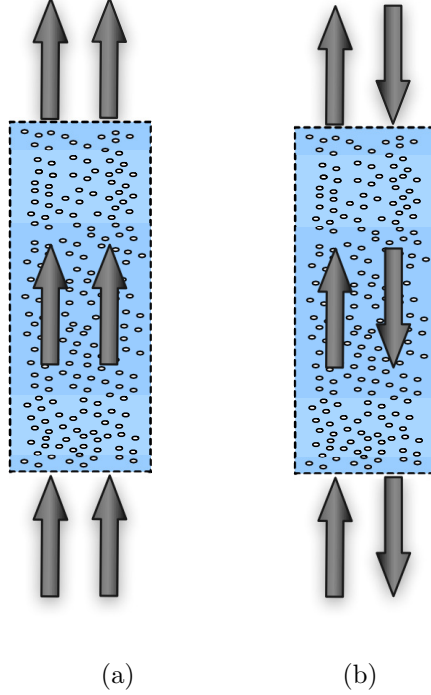


Figure 3: The two-phase flow in the bubble column reactor with open boundaries operating in two regimes: (a) co-current and (b) counter-current.

### 3.2 Pressure recovery

In the previous section, we studied the gas and liquid velocities in the quasi steady-state regime. Here, we will return to the momentum equations (3) and (4) to define the pressure in the quasi steady-state regime. Due to the fact that the model is obtained after a few simplification steps, in order to recover the pressure term in the steady-state regime, we have to consider (3) and (4) for  $\frac{\partial v_g}{\partial t} = 0$  and  $\frac{\partial v_l}{\partial t} = 0$  which are given by

$$\alpha_g v_g \rho_g \frac{\partial v_g}{\partial x} + \alpha_g \frac{dp}{dx} = -\alpha_g \rho_g g - \beta (v_g - v_l), \quad (27)$$

and

$$\alpha_l v_l \rho_l \frac{\partial v_l}{\partial x} + \alpha_l \frac{dp}{dx} - C_p \rho_l (v_g - v_l)^2 \frac{\partial \alpha_g}{\partial x} = -\alpha_l \rho_l g + \beta (v_g - v_l). \quad (28)$$

Adding (27) and (28), the pressure gradient can be calculated directly as

$$\frac{dp}{dx} = -\alpha_g v_g \rho_g \frac{\partial v_g}{\partial x} - \alpha_l v_l \rho_l \frac{\partial v_l}{\partial x} + C_p \rho_l (v_g - v_l)^2 \frac{\partial \alpha_g}{\partial x} - (\alpha_g \rho_g + \alpha_l \rho_l) g, \quad (29)$$

for the steady-state solution, and

$$\frac{dp}{dx} = -(\alpha_g \rho_g + \alpha_l \rho_l) g,$$

for the quasi steady-state where  $\alpha_g = \text{const.}$  As expected, the pressure in the quasi steadiness equals a hydrostatic pressure. Equation (29) has a form similar to the Bernoulli equation

written for the two-phase flow model [2]. To prove this statement, we can set  $\alpha_g = 1$  in (29) for the single-phase flow, which gives the following relation between the pressure and the gas velocity

$$\frac{dp}{dx} = -v_g \rho_g \frac{\partial v_g}{\partial x} - \rho_g g. \quad (30)$$

Equation (30) represents the Bernoulli equation for the single-phase flow [17]. This verifies that our modeling assumptions introduced in Section 2 are well-posed.

## 4 Causal structures in PDE systems

### 4.1 Input/output structures

In a control design, one of the first modeling concepts for causal systems is developed in the frequency domain using the Laplace transformations. As discussed in Section 2.3, the Laplace representation of PDE models can also be efficiently used to choose a causal input/output structure between quantities at the boundaries, i.e., any location in space. Applying the Laplace transformation to the model (26) yields

$$s \begin{bmatrix} W'_1(s, x) \\ W'_2(s, x) \end{bmatrix} + \begin{bmatrix} \lambda_1 & 0 \\ 0 & \lambda_2 \end{bmatrix} \frac{\partial}{\partial x} \begin{bmatrix} W'_1(s, x) \\ W'_2(s, x) \end{bmatrix} = \begin{bmatrix} c_{11} & c_{12} \\ c_{21} & c_{22} \end{bmatrix} \begin{bmatrix} W'_1(s, x) \\ W'_2(s, x) \end{bmatrix}, \quad (31)$$

which can be reordered so as to provide a set of ODEs parametrized by the Laplace variable  $s$  in the space coordinate  $x$

$$\frac{d}{dx} \begin{bmatrix} W'_1(s, x) \\ W'_2(s, x) \end{bmatrix} = \begin{bmatrix} \lambda_1 & 0 \\ 0 & \lambda_2 \end{bmatrix}^{-1} \left( \begin{bmatrix} c_{11} & c_{12} \\ c_{21} & c_{22} \end{bmatrix} - sI \right) \begin{bmatrix} W'_1(s, x) \\ W'_2(s, x) \end{bmatrix}. \quad (32)$$

The advantage of the Laplace-space representation of the two-phase flow model given by (32) is that it can be solved analytically by integrating (32) over the space. This means that the relationships between potentially chosen inputs and outputs are determined by transfer functions that link boundary conditions. The following relationship between the flow variables defined at the bottom boundary  $x = 0$  and at any location  $x > 0$  can be obtained

$$\begin{bmatrix} W'_1(s, x) \\ W'_2(s, x) \end{bmatrix} = \exp(\mathcal{A}(s)x) \begin{bmatrix} W'_1(s, 0) \\ W'_2(s, 0) \end{bmatrix}, \quad (33)$$

with  $\mathcal{A}(s)$  being the system matrix parametrized by  $s$

$$\mathcal{A}(s) = \begin{bmatrix} \frac{c_{11} - s}{\lambda_1} & \frac{c_{12}}{\lambda_1} \\ \frac{c_{21}}{\lambda_2} & \frac{c_{22} - s}{\lambda_2} \end{bmatrix}. \quad (34)$$

Equation (33) directly connects the flow variable at different locations of the bubble column, which can be considered as inputs and outputs. In this case, the system dynamics are described by the system matrix  $\mathcal{A}(s)$ . The specification of appropriate inputs and outputs,

which lead to a causal input/output structure, can now be done by analyzing the eigenvalues of  $\mathcal{A}(s)$ . The causal input/output structures can be determined by decoupling the system in a similar manner as it was presented in Section 2. In contrast to the decoupling presented in Section 2.5, decoupling of (33) includes the directional derivatives  $\lambda_1$  and  $\lambda_2$  and the coupling coefficients  $c_{11}$ ,  $c_{12}$ ,  $c_{21}$ , and  $c_{22}$ . The advantage of the decoupled system is that the system dynamics can be fully decoupled preserving the dynamics described by the eigenvalues of the system matrix  $\mathcal{A}(s)$ . The coordinates  $\mathbf{W}'(s, x)$  can be transformed to the new coordinate system  $\mathbf{Z}'(s, x)$  using the following general expression

$$\mathbf{Z}'(s, x) = \mathbf{Q}(s)\mathbf{W}'(s, x), \quad (35)$$

where  $\mathbf{Q}(s)$  represents the transformation matrix which contains the eigenvectors corresponding to the eigenvalues of  $\mathcal{A}(s)$  in the right order, i.e.,

$$\mathbf{Q}(s) = \begin{bmatrix} q_{11}(s) & q_{12}(s) \\ q_{21}(s) & q_{22}(s) \end{bmatrix},$$

with the following elements

$$\begin{aligned} q_{11}(s) &= 1, & q_{12}(s) &= \frac{1}{2c_{21}\lambda_1} \left( \lambda_2 c_{11} - \lambda_1 c_{22} + (-\lambda_2 + \lambda_1)s + \sqrt{\mu(s)} \right), \\ q_{21}(s) &= 1, & q_{22}(s) &= -\frac{1}{2c_{21}\lambda_1} \left( -\lambda_2 c_{11} + \lambda_1 c_{22} - (-\lambda_2 + \lambda_1)s + \sqrt{\mu(s)} \right), \end{aligned}$$

where

$$\mu(s) = ((\lambda_1 - \lambda_2)s + (c_{11}\lambda_2 - \lambda_1 c_{22}))^2 + 4\lambda_1\lambda_2 c_{21}. \quad (36)$$

Note that the elements  $q_{12}(s)$  and  $q_{22}(s)$  are irrational functions since they are functions of  $\sqrt{\mu(s)}$ .

Using the coordinate transformation (35), the fully decoupled system in the new coordinate system  $\mathbf{Z}'(s, x)$  can be written as

$$\begin{bmatrix} Z'_1(s, x) \\ Z'_2(s, x) \end{bmatrix} = \begin{bmatrix} e^{\lambda_1^*(s)x} & 0 \\ 0 & e^{\lambda_2^*(s)x} \end{bmatrix} \begin{bmatrix} Z'_1(s, 0) \\ Z'_2(s, 0) \end{bmatrix}. \quad (37)$$

Then, the eigenvalues of  $\mathcal{A}(s)$  can be obtained from the following expression

$$\lambda_1^*(s) = \frac{1 - (\lambda_1 + \lambda_2)s + \lambda_1 c_{22} + \lambda_2 c_{11} + \sqrt{\mu(s)}}{2\lambda_1\lambda_2}, \quad (38)$$

$$\lambda_2^*(s) = \frac{1 - (\lambda_1 + \lambda_2)s + \lambda_1 c_{22} + \lambda_2 c_{11} - \sqrt{\mu(s)}}{2\lambda_1\lambda_2}. \quad (39)$$

The signs of the eigenvalues  $\lambda_1^*(s)$  and  $\lambda_2^*(s)$  determine the causality of the input/output structure for the linearized two-phase flow system. Different input/output structures are possible according to the signs of  $\lambda_1^*(s)$  and  $\lambda_2^*(s)$ . Table 2 outlines four different cases.

For example, suppose that  $\lambda_1^*(s) < 0$  and  $\lambda_2^*(s) < 0$  for all  $s$  (case 1 in Table 2), then the inputs have to be defined at  $x = 0$  and the outputs at  $x = L$  as illustrated in Figure 4(a). Then, according to (37), the connections between the inputs  $Z'_1(s, 0)$  and  $Z'_2(s, 0)$

Table 2: Wave propagation and input/output structures based on the eigenvalue analysis in the Laplace-space domain in the  $\mathbf{Z}'(s, x)$  coordinate system.

Case	Eigenvalues of the system parametrized by $s$	Inputs	Outputs
1	$\lambda_1^*(s) < 0$ $\lambda_2^*(s) < 0$	$\begin{bmatrix} Z'_1(s, 0) \\ Z'_2(s, 0) \end{bmatrix}$	$\begin{bmatrix} Z'_1(s, L) \\ Z'_2(s, L) \end{bmatrix}$
2	$\lambda_1^*(s) > 0$ $\lambda_2^*(s) < 0$	$\begin{bmatrix} Z'_1(s, L) \\ Z'_2(s, 0) \end{bmatrix}$	$\begin{bmatrix} Z'_1(s, 0) \\ Z'_2(s, L) \end{bmatrix}$
3	$\lambda_1^*(s) < 0$ $\lambda_2^*(s) > 0$	$\begin{bmatrix} Z'_1(s, 0) \\ Z'_2(s, L) \end{bmatrix}$	$\begin{bmatrix} Z'_1(s, L) \\ Z'_2(s, 0) \end{bmatrix}$
4	$\lambda_1^*(s) > 0$ $\lambda_2^*(s) > 0$	$\begin{bmatrix} Z'_1(s, L) \\ Z'_2(s, L) \end{bmatrix}$	$\begin{bmatrix} Z'_1(s, 0) \\ Z'_2(s, 0) \end{bmatrix}$

and the outputs  $Z'_1(s, L)$  and  $Z'_2(s, L)$  are defined by the delay functions  $e^{\lambda_1^*(s)L}$  and  $e^{\lambda_2^*(s)L}$ , respectively, i.e.,

$$\begin{bmatrix} Z'_1(s, L) \\ Z'_2(s, L) \end{bmatrix} = \begin{bmatrix} e^{\lambda_1^*(s)L} & 0 \\ 0 & e^{\lambda_2^*(s)L} \end{bmatrix} \begin{bmatrix} Z'_1(s, 0) \\ Z'_2(s, 0) \end{bmatrix}. \quad (40)$$

Suppose now that  $\lambda_1^*(s) > 0$  and  $\lambda_2^*(s) < 0$  (case 2 in Table 2), then the first equation in (37) is the inverse of a time delay function which is not physically realizable. In terms of dynamics, (37) represents a non-causal relationship between  $Z'_1(s, 0)$  and  $Z'_1(s, L)$ . This means that the wave with  $\lambda_1^*(s) > 0$  propagates in the opposite direction to the predicted direction, i.e., from top to bottom. By reordering (40), the system can be put into a causal input/output form that follows the direction of the wave propagation, i.e.,

$$\begin{bmatrix} Z'_1(s, 0) \\ Z'_2(s, L) \end{bmatrix} = \begin{bmatrix} e^{-\lambda_1^*(s)L} & 0 \\ 0 & e^{\lambda_2^*(s)L} \end{bmatrix} \begin{bmatrix} Z'_1(s, L) \\ Z'_2(s, 0) \end{bmatrix}. \quad (41)$$

This inversion of the relationship between the input  $Z'_1(s, L)$  and the output  $Z'_1(s, 0)$  renders the set of equations (41) into a causal form. Figure 4(b) illustrates the inversion which implies that the resulting system is bilaterally coupled [26]. As illustrated in Figure 4, the causal input/output structures between the properties at the boundaries can be viewed as an extension of the system boundaries to their surroundings.

As already discussed in Section 2, a simple coordinate transformation allows us to transform a PDE model from one coordinate system to another by applying the inverse of the transformation matrix (see Section 2.5). However, a coordinate transformation for PDE models in the Laplace-space domain is a bit more involved. In the remainder of this section, we will present two coordinate transformations for the two-phase flow model (33) for: the co-current flow (see Figure 4(a)) and the counter-current flow (see Figure 4(b)).

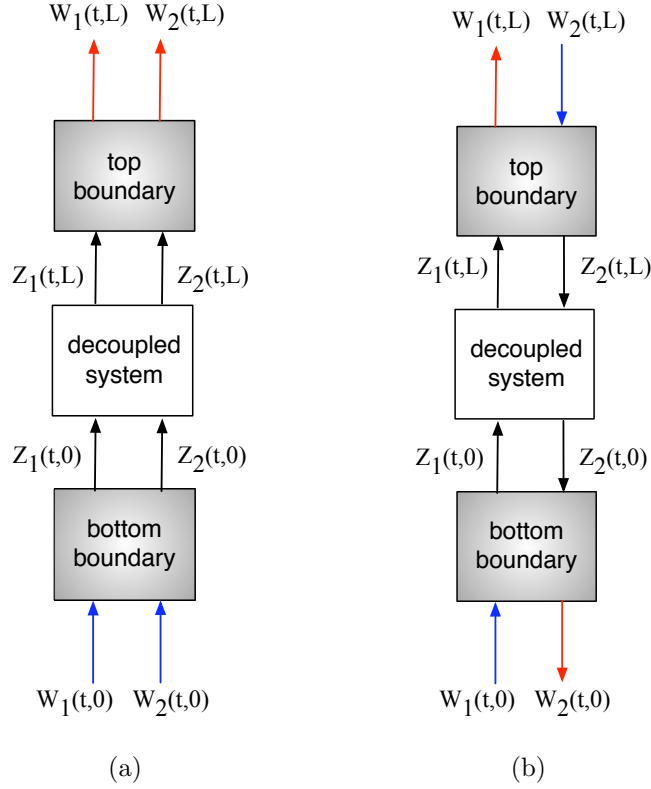


Figure 4: Input/output structures for (a) a co-current flow and (b) a counter-current flow. The blue arrows represent inputs, whereas the red arrows represent the outputs.

The coordinate transformation for the co-current flow as illustrated in Figure 4(a) and for the counter-current flow as illustrated in Figure 4(b) can be recovered using the following relationship

$$\begin{bmatrix} W'_1(s, x) \\ W'_2(s, x) \end{bmatrix} = \mathbf{Q}^{-1}(s) \begin{bmatrix} Z'_1(s, x) \\ Z'_2(s, x) \end{bmatrix}. \quad (42)$$

- **Co-current flow**

The following model representation in the  $\mathbf{W}'(s, x)$  coordinates can be obtained on basis of the actuation strategy given in Figure 4(a)

$$\begin{bmatrix} W'_1(s, L) \\ W'_2(s, L) \end{bmatrix} = \mathbf{G}_{\text{co}}(s) \begin{bmatrix} W'_1(s, 0) \\ W'_2(s, 0) \end{bmatrix}, \quad (43)$$

where

$$\mathbf{G}_{\text{co}}(s) = \mathbf{Q}^{-1}(s) \begin{bmatrix} e^{\lambda_1^*(s)x} & 0 \\ 0 & e^{\lambda_2^*(s)x} \end{bmatrix} \mathbf{Q}(s).$$

- **Counter-current flow**

Figure 4(b) shows the way to recover the  $\mathbf{W}'(s, x)$  coordinates for the counter-current flow. The bottom boundary can be recovered as

$$\begin{bmatrix} Z'_1(s, 0) \\ W'_2(s, 0) \end{bmatrix} = \begin{bmatrix} q_{11}(s) - \frac{q_{12}(s)q_{21}(s)}{q_{22}(s)} & \frac{q_{12}(s)}{q_{22}(s)} \\ -\frac{q_{21}(s)}{q_{22}(s)} & \frac{1}{q_{22}(s)} \end{bmatrix} \begin{bmatrix} W'_1(s, 0) \\ Z'_2(s, 0) \end{bmatrix}, \quad (44)$$

whereas the top boundary can be recovered as

$$\begin{bmatrix} W'_1(s, L) \\ Z'_2(s, L) \end{bmatrix} = \begin{bmatrix} \frac{1}{q_{11}(s)} & -\frac{q_{12}(s)}{q_{11}(s)} \\ \frac{q_{21}(s)}{q_{11}(s)} & q_{22}(s) - \frac{q_{12}(s)q_{21}(s)}{q_{11}(s)} \end{bmatrix} \begin{bmatrix} Z'_1(s, L) \\ W'_2(s, L) \end{bmatrix}. \quad (45)$$

Using the linear combination of the given boundaries (44) and (45), the original coordinates can be fully recovered as

$$\begin{bmatrix} W'_1(s, 0) \\ W'_2(s, L) \end{bmatrix} = \mathbf{G}_{cc}(s) \begin{bmatrix} W'_1(s, L) \\ W'_2(s, 0) \end{bmatrix}, \quad (46)$$

where

$$\mathbf{G}_{cc}(s) = \begin{bmatrix} q_{11}(s) & -q_{12}(s)e^{-\lambda_1^*(s)} \\ q_{21}(s)e^{\lambda_2^*(s)} & -q_{22}(s) \end{bmatrix}^{-1} \begin{bmatrix} q_{11}e^{-\lambda_1^*(s)} & -q_{12}(s) \\ q_{21}(s) & -q_{22}(s)e^{\lambda_2^*(s)} \end{bmatrix}.$$

Equation (46) represents a causal input/output structure between the properties at the boundaries, where the system dynamics are described by the elements of  $\mathbf{G}_{cc}(s)$ .

The functional relationships (43) and (46) are algebraic representations of the two-phase flow model using the Laplace transformation. Due to the simple algebraic expressions  $\mathbf{G}_{co}(s)$  and  $\mathbf{G}_{cc}(s)$ , the behavior of the system between the boundaries in the Laplace-space domain can be easily simulated with a little computational effort. In general, a rational transfer function has many useful interpretations and features which are often associated with important system properties and control designs. The computational complexity associated with the complex CFD models of two-phase flow and control of such models can be greatly simplified by making use of the theory associated with the rational transfer functions and the Padé approximations. The simulation time required for rational transfer functions in Matlab is just a few seconds compared to CFD models. This is a huge advantage of the Laplace-space representation of the two-phase flow model.

## 5 Boundary control design

The main control objective is to stabilize the flow around the quasi steady-state and suppress any fluctuation caused by disturbances or secondary flow. This control objective can be achieved by a unique input/output strategy and boundary control design. For a laminar flow regime which is characterized by less drag force between the phases, the flow can be stabilized around the laminar flow applying a controller at the boundaries. Enhancement of the plug

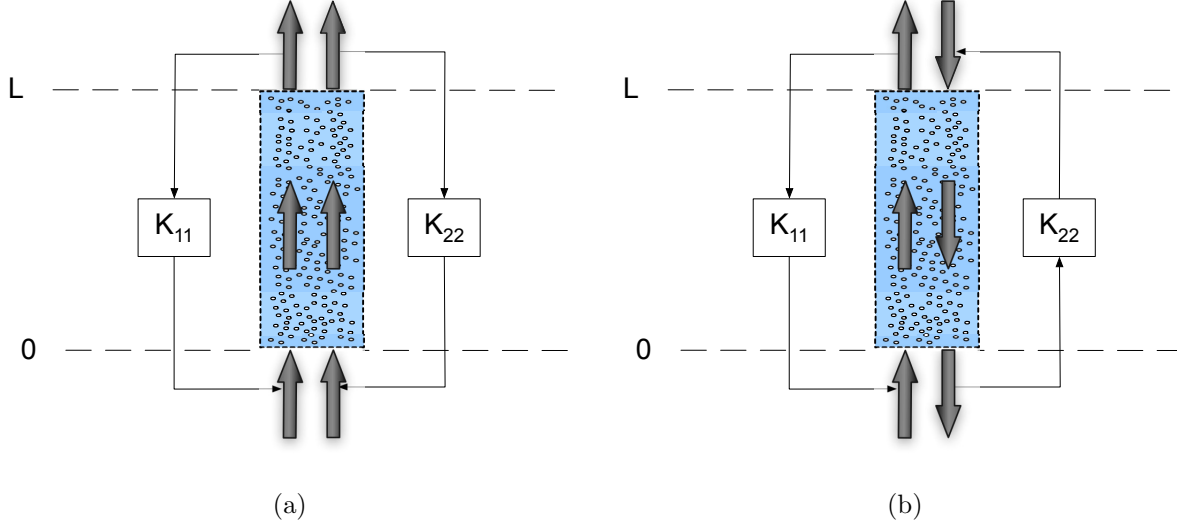


Figure 5: Boundary control strategies for the two-phase flow model for (a) co-current and (b) counter-current flow.

flow regime in the laminar two-phase flow inside a bubble column can be easily obtained by introducing more valves at the boundaries and using a more powerful pump/compressor equipment.

Using the derived two-phase flow model in the Laplace-space representation (33), the boundary control law can be derived using the following conditions for:

1. Co-current flow

$$\begin{bmatrix} W_1(s, L) \\ W_2(s, L) \end{bmatrix} = \begin{bmatrix} K_{11} & 0 \\ 0 & K_{22} \end{bmatrix} \begin{bmatrix} W_1(s, 0) \\ W_2(s, 0) \end{bmatrix}, \quad (47)$$

2. Counter-current flow

$$\begin{bmatrix} W_1(s, 0) \\ W_2(s, L) \end{bmatrix} = \begin{bmatrix} K_{11} & 0 \\ 0 & K_{22} \end{bmatrix} \begin{bmatrix} W_1(s, L) \\ W_2(s, 0) \end{bmatrix}. \quad (48)$$

The boundary conditions (47) and (48) contain the tunable control parameters  $K_{11}$  and  $K_{22}$  illustrated in Figure 5 that can control the two-phase flow in a desirable manner ensuring stabilization of the specific flow regimes.

## 5.1 Numerical example

In this section, we give simulation results of an uncontrolled and controlled two-phase flow based on the derived two-phase flow model given as (37) for the counter-current flow illustrated in Figure 5(b). For air/water system with  $\bar{\alpha}_g = 0.1$ ,  $\bar{v}_g = 0.155$ , and  $\bar{v}_l = -0.017$ , according to the discussion presented in Section 3 the slip velocity  $v_s = 0.17$ . Following the theoretical framework given in Sections 2.4 and 2.5, the system parameters of the linearized

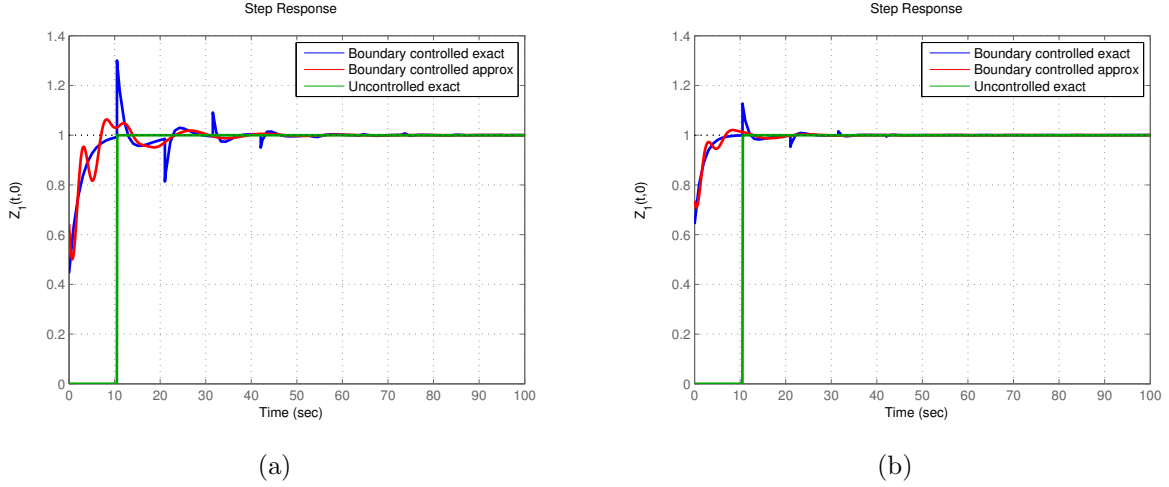


Figure 6: Step responses for an uncontrolled and controlled flow with the proportional gain  $K_{11} = 0.3$  for the exact and approximate solutions of the controlled flow using a fourth-order Padé approximation.

two-phase flow model written as (26) can be easily computed. The values of the system parameters are given in Table 3.

Table 3: Fluid properties and system parameters.

Symbol	Value
$\lambda_1$	0.0954
$\lambda_2$	-0.064
$c_{11}$	521
$c_{12}$	1647
$c_{21}$	-521
$c_{22}$	-1647

As shown in Figure 4(b) for counter-current flow, the top and bottom boundary blocks represent the coordinate transformations between the coordinates which can be recovered following the causal flow directions. The exponential functions, which represent the transportation delays characterized by the eigenvalues  $\lambda_1^*(s)$  and  $\lambda_2^*(s)$ , can be approximated by rational transfer functions  $\mathbf{G}_{cc}(s)$  for the counter-current flow. In order to understand possible means of the complex eigenvalues and check the causality requirement given in Section 4, we use the Padé approximations of the eigenvalues  $\lambda_1^*(s)$  and  $\lambda_2^*(s)$ . In the example shown in Figure 6, we use a fourth-order Padé approximation of the eigenvalue  $\lambda_1^*(s)$ . Figure 6 compares the uncontrolled and controlled flow with the exact solution and approximate solution. The exact solution is replaced by a Padé approximation.

As can be seen, the boundary controller for the upward propagation can push the flow faster from one side of the boundary to the other side with fluctuations that fade out with re-

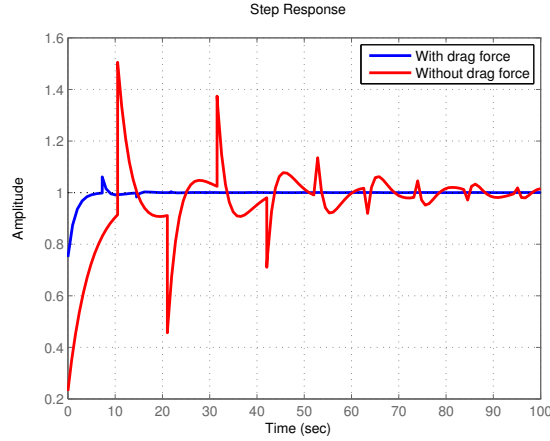


Figure 7: The time responses of the controlled flow with and without the drag force for the wave that propagates from the bottom.

spect to time. The fluctuations are mainly caused by the drag force which can be suppressed by tuning  $K_{11}$  for the internal delay function as illustrated in Figure 4(b). The plug flow that is created in this way has to travel with the shortest possible time from one boundary to the other boundary. This means that the controller has to place the eigenvalue  $\lambda_1^*(s)$  closer to zero, since this would mean that there is almost no delay of the fluid properties between the boundaries. Figure 6(b) shows the control results obtained applying the proportional gain  $K_{11}$  at the boundaries that can achieve this goal. As can be seen, the controller  $K_{11}$  influences the internal delay of the flow between the properties at the bottom and top boundaries, forming flow oscillations according to the magnitude of  $K_{11}$ . The oscillations of the flow should be as small as possible in order to keep the flow close to the plug flow regime. Furthermore, the plug flow regime that is created in this way has the shortest traveling time of the two-phase flow from one boundary to the other. This means that the control objective is to place the eigenvalues  $\lambda_1^*(s)$  and  $\lambda_2^*(s)$  closer to zero. The zero eigenvalues represent the flow without the delays  $e^{-\lambda_1^*(s)L}$  and  $e^{\lambda_2^*(s)L}$  of the two-phase flow between the boundaries. Due to the fact that the value  $e^{\lambda_2^*(s)L}$  is rather small, the effect of the flow in the opposite direction can be neglected.

To demonstrate the effectiveness of the boundary controller, we also compare the controlled flow with the drag force and without the drag force. Figure 7 illustrates the simulation results. As can be seen, the proposed boundary controller minimizes the effect of the drag force almost completely. Although we present the numerical results obtained by applying a unity step, which is unlikely to happen in reality for the two-phase flow, the results show the system dynamics of the two-phase flow model and influence of the controllers on the dynamics. The input can be easily scaled in the control design in order to described the real injections and suction throughout the valves for different practical setups.

## 6 Conclusions

In this paper, we have presented a control-oriented two-phase flow model with a theoretical framework for a boundary control of the two-phase flow system. The given framework establishes the analysis of causal input/output structures for two-phase flow systems, and proposes a new modeling approach based on the Laplace-space representation of the derived two-phase flow model. The main advantage of the Laplace-space approach is that it fully determines the causality of the input/output structures for a wide range of operating regimes, and it provides insights needed for the boundary control design. The implementation of the proposed boundary control design involves the actuation of the flow at different locations according to the flow regimes. The control action at the boundaries means suction and injection of the fluid into the system. The injection/suction at the boundaries particularly affects the shape of the velocity profile near the boundaries and changes the flow regime. The benefits that can be gained from the boundary control include the reduction of the influence of the drag force in the fluid flow. The proposed boundary control design can reduce the residence time of the flow between the top and bottom boundary of the column and can suppress the fluctuations at the boundaries, which can be seen as a delay. Applying a small gain at the boundaries, the delay can be considerably reduced with a small fluctuation of the fluid flow. The main contribution of the paper includes an implementable boundary controller for a uniform flow regime of the two-phase flow in the vertical bubble column that can be extended for more complex flow cases.

## References

- [1] O.M. Aamo and M. Krstić. *Flow control by feedback: stabilization and mixing*. Springer Verlag, 2003.
- [2] J.D. Anderson and J.F. Wendt. *Computational fluid dynamics*. McGraw-Hill New York, 1995.
- [3] T.R. Bewley. Flow control: new challenges for a new renaissance. *Progress in Aerospace Sciences*, 37(1):21–58, 2001.
- [4] A. Biesheuvel and L. Wijngaarden. Two-phase flow equations for a dilute dispersion of gas bubbles in liquid. *Journal of Fluid Mechanics*, 148:301–18, 1984.
- [5] J.C. Charpentier. Modern chemical engineering in the framework of globalization, sustainability, and technical innovation. *Industrial & Engineering Chemistry Research*, 46(11):3465–3485, 2007.
- [6] P.D. Christofides. *Nonlinear and robust control of PDE systems: methods and applications to transport-reaction processes*. Birkhauser, 2001.
- [7] P.D. Christofides and P. Daoutidis. Feedback control of hyperbolic PDE systems. *AIChE Journal*, 42(11):3063–3086, 1996.
- [8] R. D’Andrea and G.E. Dullerud. Distributed control design for spatially interconnected systems. *IEEE Transactions on Automatic Control*, 48(9):1478–1495, 2003.

- [9] D.C. Dankworth and S. Sundaresan. Time-dependent vertical gas-liquid flow in packed beds. *Chemical Engineering Science*, 47:337–46, 1992.
- [10] J. De Halleux, C. Prieur, J.M. Coron, B. d’Andrea Novel, and G. Bastin. Boundary feedback control in networks of open channels. *Automatica*, 39(8):1365–1376, 2003.
- [11] W.-D. Deckwer. *Bubble column reactors*. Wiley, 1992.
- [12] D. Del Vecchio and N. Petit. Boundary control for an industrial under-actuated tubular chemical reactor. *Journal of Process Control*, 15(7):771–784, 2005.
- [13] S Djordjevic. *Modeling and control perspectives of two-phase fluid systems*. PhD thesis, Delft University of Technology, The Netherlands, 2011.
- [14] S. Djordjevic, O.H. Bosgra, P.M.J. Van den Hof, and D. Jeltsema. Boundary actuation structure of linearized two-phase flow. In *Proceedings of the American Control Conference 2010*, pages 3759–3764, 2010.
- [15] D.A. Drew. Mathematical modeling of two-phase flow. *Annual review of fluid mechanics*, 15(1):261–291, 1983.
- [16] S.D. Gharat and J.B. Joshi. Transport phenomena in bubble column reactors I: Flow pattern. *The Chemical Engineering Journal*, 48(3):141–151, 1992.
- [17] M. Ishii and T. Hibiki. *Thermo-fluid dynamics of two-phase flow*. Springer, 2006.
- [18] H.A. Jakobsen, B.H. Sannæs, S. Grevskott, and H.F. Svendsen. Modeling of bubble driven vertical flows. *Industrial & Engineering Chemistry Research*, 36:4052–4074, 1997.
- [19] J.B. Joshi. Computational flow modelling and design of bubble column reactors. *Chemical Engineering Science*, 56:5893–5933, 2001.
- [20] M.R. Jovanovic and B. Bamieh. Componentwise energy amplification in channel flows. *Journal of Fluid Mechanics*, 534:145–183, 2005.
- [21] M. Krstic and A. Smyshlyaev. Backstepping boundary control for first-order hyperbolic PDEs and application to systems with actuator and sensor delays. *Systems & Control Letters*, 57(9):750–758, 2008.
- [22] X. Litrico and V. Fromion. Boundary control of hyperbolic conservation laws using a frequency domain approach. *Automatica*, 45(3):647–656, 2009.
- [23] A. Maidi, M. Diaf, and J.P. Corriou. Boundary control of a parallel-flow heat exchanger by input-output linearization. *Journal of Process Control*, 2010.
- [24] J.A. Moulijn, A. Stankiewicz, J. Grievink, and A. Gorak. Process intensification and process systems engineering: A friendly symbiosis. *Computers & Chemical Engineering*, 32(1-2):3–11, 2008.

- [25] J.W. Park, D.A. Drew, and R.T. Lahey, Jr. The analysis of void wave propagation in adiabatic monodispersed bubbly two-phase flows using an ensemble-averaged two-fluid model. *International Journal of Multiphase Flow*, 24(7):1205–1244, 1999.
- [26] H.M. Paynter. *Analysis and design of engineering systems*. MIT press Cambridge, Mass., 1961.
- [27] M.A. Pinsky and A. Gray. *Partial differential equations and boundary-value problems with applications*. McGraw-Hill New York, 1991.
- [28] V.H. Ransom and D.L. Hicks. Hyperbolic two-pressure models for two-phase flow. *Journal of Computational Physics*, 53(1):124–151, 1984.
- [29] H. Sano. Exponential stability of a mono-tubular heat exchanger equation with output feedback. *Systems & Control Letters*, 50(5):363–369, 2003.
- [30] H. Stadtke. *Gasdynamic aspects of two-phase Flow : hyperbolicity, wave propagation phenomena, and related numerical methods*. Wiley-VCH, 2006.
- [31] T. Van Gerven and A. Stankiewicz. Structure, energy, synergy, time: the fundamentals of process intensification. *Industrial & Engineering Chemistry Research*, 48(2):814–826, 2009.
- [32] W. Waldruff, D. Dochain, S. Bourrel, and A. Magnus. On the use of observability measures for sensor location in tubular reactor. *Journal of Process Control*, 8(5-6):497–505, 1998.

## Appendix A

First, we start with the two-phase flow model (1), (5) and (6), where (17) is inserted for each state separately

$$\begin{aligned}
& \frac{\partial(\bar{\alpha}_g + \alpha'_g)}{\partial t} + \frac{\partial(\bar{\alpha}_g + \alpha'_g)}{\partial x}(\bar{v}_g + v'_g) + (\bar{\alpha}_g + \alpha'_g) \frac{\partial(\bar{v}_g + v'_g)}{\partial x} = 0, \\
& \rho_g \frac{\partial(\bar{v}_g + v'_g)}{\partial t} - \rho_l \frac{\partial(\bar{v}_l + v'_l)}{\partial t} + \rho_g(\bar{v}_g + v'_g) \frac{\partial(\bar{v}_g + v'_g)}{\partial x} - \rho_l(\bar{v}_l + v'_l) \frac{\partial(\bar{v}_l + v'_l)}{\partial x} \\
& \quad + C_p \rho_l ((\bar{v}_g + v'_g) - (\bar{v}_l + v'_l))^2 \frac{\partial(\bar{\alpha}_g + \alpha'_g)}{\partial x} \\
& \quad = -(\rho_g - \rho_l)g - ((\bar{v}_g + v'_g) - (\bar{v}_l + v'_l)) \frac{3}{4} \frac{C_d}{d_b} \sqrt{((\bar{v}_g + v'_g) - (\bar{v}_l + v'_l))^2}, \\
& \frac{\partial(\bar{\alpha}_g + \alpha'_g)}{\partial x} ((\bar{v}_g + v'_g) - (\bar{v}_l + v'_l)) + \frac{\partial(\bar{v}_g + v'_g)}{\partial x} (\bar{\alpha}_g + \alpha'_g) \\
& \quad + (1 - (\bar{\alpha}_g + \alpha'_g)) \frac{\partial(\bar{v}_l + v'_l)}{\partial x} = 0.
\end{aligned}$$

Notice that the drag force is simplified using the following relation

$$\alpha_g \alpha_l \left( \frac{1}{\alpha_g} + \frac{1}{\alpha_l} \right) = 1.$$

Now, we can evaluate each equation separately in order to obtain the linearized two-phase flow model, which can be written as

$$\frac{\partial \bar{\alpha}_g}{\partial t} + \frac{\partial \bar{\alpha}_g}{\partial x} \bar{v}_g + \bar{\alpha}_g \frac{\partial \bar{v}_g}{\partial x} = 0,$$

where  $\alpha'_g \frac{\alpha'_g}{\partial x} \approx 0$  for the perturbation in the vicinity of the steady-state solution, i.e.,

$$\frac{\partial \alpha'_g}{\partial t} + \frac{\partial \alpha'_g}{\partial x} \bar{v}_g + \bar{\alpha}_g \frac{\partial v'_g}{\partial x} + \frac{\partial \bar{\alpha}_g}{\partial x} v'_g + \alpha'_g \frac{\partial \bar{v}_g}{\partial x} = 0. \quad (49)$$

Equation (49) is the linearized mass equation which accounts the variation of the steady-state solution with respect to space  $\frac{\partial \bar{\alpha}_g}{\partial x} v'_g$  and  $\alpha'_g \frac{\partial \bar{v}_g}{\partial x}$ . If the steady-state solution is space-independent, the linearized mass equation equals

$$\frac{\partial \alpha'_g}{\partial t} + \frac{\partial \alpha'_g}{\partial x} \bar{v}_g + \bar{\alpha}_g \frac{\partial v'_g}{\partial x} = 0.$$

In contrast to the linearization of the mass equation, the linearization of the momentum equation is more computationally involved due to the nonlinear interfacial pressure and the drag force

$$\begin{aligned} & \rho_g \frac{\partial (\bar{v}_g + v'_g)}{\partial t} - \rho_l \frac{\partial (\bar{v}_l + v'_l)}{\partial t} + \rho_g (\bar{v}_g + v'_g) \frac{\partial (\bar{v}_g + v'_g)}{\partial x} - \rho_l (\bar{v}_l + v'_l) \frac{\partial (\bar{v}_l + v'_l)}{\partial x} \\ & + C_p \rho_l ((\bar{v}_g + v'_g) - (\bar{v}_l + v'_l))^2 \frac{\partial (\bar{\alpha}_g + \alpha'_g)}{\partial x} \\ & = -(\rho_g - \rho_l)g - ((\bar{v}_g + v'_g) - (\bar{v}_l + v'_l)) \frac{3 C_d}{4 d_b} \sqrt{((\bar{v}_g + v'_g) - (\bar{v}_l + v'_l))^2}, \end{aligned}$$

$$\begin{aligned} & \rho_g \frac{\partial \bar{v}_g}{\partial t} - \rho_l \frac{\partial \bar{v}_l}{\partial t} + \rho_g \bar{v}_g \frac{\partial \bar{v}_g}{\partial x} - \rho_l \bar{v}_l \frac{\partial \bar{v}_l}{\partial x} + C_p \rho_l (\bar{v}_g - \bar{v}_l)^2 \frac{\partial \bar{\alpha}_g}{\partial x} \\ & = -(\rho_g - \rho_l)g - (\bar{v}_g - \bar{v}_l) \frac{3 C_d}{4 d_b} \sqrt{(\bar{v}_g - \bar{v}_l)^2}. \end{aligned}$$

The linearized momentum equation is given by

$$\begin{aligned} & \rho_g \frac{\partial v'_g}{\partial t} - \rho_l \frac{\partial v'_l}{\partial t} + \rho_g \bar{v}_g \frac{\partial v'_g}{\partial x} + \rho_g v'_g \frac{\partial \bar{v}_g}{\partial x} - \rho_l \bar{v}_l \frac{\partial v'_l}{\partial x} - \rho_l v'_l \frac{\partial \bar{v}_l}{\partial x} \\ & + C_p \rho_l (\bar{v}_g - \bar{v}_l)^2 \frac{\partial \alpha'_g}{\partial x} + C_p \rho_l (v'_g - v'_l)^2 \frac{\partial \alpha'_g}{\partial x} \\ & + 2C_p \rho_l (\bar{v}_g - \bar{v}_l) (v'_g - v'_l) \frac{\partial \alpha'_g}{\partial x} \\ & + C_p \rho_l (v'_g - v'_l)^2 \frac{\partial \bar{\alpha}_g}{\partial x} + 2C_p \rho_l (\bar{v}_g - \bar{v}_l) (v'_g - v'_l) \frac{\partial \bar{\alpha}_g}{\partial x} \\ & = -\frac{3 C_d}{4 d_b} (v'_g - v'_l)^2 - 2\frac{3 C_d}{4 d_b} (\bar{v}_g - \bar{v}_l) (v'_g - v'_l). \end{aligned}$$

Note that the terms  $(v'_g - v'_l)^2 \frac{\partial \alpha'_g}{\partial x} \approx 0$ ,  $(v'_g - v'_l) \frac{\partial \alpha'_g}{\partial x} \approx 0$ , and  $(v'_g - v'_l)^2 \approx 0$ , thus the final form of the linearized momentum equation is

$$\begin{aligned} & \rho_g \frac{\partial v'_g}{\partial t} - \rho_l \frac{\partial v'_l}{\partial t} + \rho_g \bar{v}_g \frac{\partial v'_g}{\partial x} + \rho_g v'_g \frac{\partial \bar{v}_g}{\partial x} - \rho_l \bar{v}_l \frac{\partial v'_l}{\partial x} - \rho_l v'_l \frac{\partial \bar{v}_l}{\partial x} \\ & + C_p \rho_l (\bar{v}_g - \bar{v}_l)^2 \frac{\partial \alpha'_g}{\partial x} + 2C_p \rho_l (\bar{v}_g - \bar{v}_l) (v'_g - v'_l) \frac{\partial \bar{\alpha}_g}{\partial x} \\ & = -2 \frac{3}{4} \frac{C_d}{d_b} \sqrt{(\bar{v}_g - \bar{v}_l)^2} (v'_g - v'_l). \end{aligned}$$

Finally, we linearize the algebraic part of the two-phase flow model suggested in Section 2.4. The linearized algebraic equation can be written in terms of perturbations as

$$\begin{aligned} & \frac{\partial(\bar{\alpha}_g + \alpha'_g)}{\partial x} ((\bar{v}_g + v'_g) - (\bar{v}_l + v'_l)) + \frac{\partial(\bar{v}_g + v'_g)}{\partial x} (\bar{\alpha}_g + \alpha'_g) \\ & + (1 - (\bar{\alpha}_g + \alpha'_g)) \frac{\partial(\bar{v}_l + v'_l)}{\partial x} = 0. \end{aligned} \quad (50)$$

The final form of the linearized algebraic equation (50) can be obtained from the following equation

$$\frac{\partial \bar{\alpha}_g}{\partial x} (v'_g - v'_l) + \frac{\partial \alpha'_g}{\partial x} (\bar{v}_g - \bar{v}_l) + \frac{\partial \bar{v}_g}{\partial x} \alpha'_g + \frac{\partial v'_g}{\partial x} \bar{\alpha}_g + (1 - \bar{\alpha}_g) \frac{\partial v'_l}{\partial x} - \alpha'_g \frac{\partial \bar{v}_l}{\partial x} = 0.$$

Now, by letting  $\Phi' = [ \alpha'_g \quad v'_g \quad v'_l ]^T$  we can obtain the compact form witten as (18).